Supporting Information

Crack-free hematite inverse opal photo-anodes for enhancing photo-electrochemical water splitting

Heling Zhu,[a] Yajuan Zhang,[a] Jingqian Zhu,[a] Yuhuan Li, [a] Saihua Jiang,[b] Na Wu,[a] Yu Wei,[a] Jinming Zhou,[a,b] and Yanlin Song[c]

[a]Key Laboratory of Inorganic Nanomaterials of Hebei Province,
College of Chemistry and Material Science,
Hebei Normal University, Shijiazhuang, Hebei 050024 P. R. China
E-mail: zhoujm@iccas.ac.cn

[b]Department of Materials Science & Engineering,
University of Pennsylvania, Philadelphia, PA 19104
[c]Key Laboratory of Green Printing, Institute of Chemistry,
Chinese Academy of Sciences, Beijing, 100190 P. R. China
E-mail: ylsong@iccas.ac.cn

KEYWORDS. inverse opals, photonic bandgap, hematite photo-anodes, crack-free, photo-electrochemical water splitting

Experimental section

Fabrication of the crack-free hematite inverse opals photo-anodes:

The monodisperse poly(styrene-methyl methacrylate-acrylic acid) [P(St-MMA-AA)] latex nanospheres with controlled sizes were synthesized by a one-step emulsion polymerization method.[S1] The opal colloidal crystal templates were self-assembled onto FTO glass through vertical deposition at a constant temperature of 60 ^{o}C and relative humidity of 60%.[S1] The templates were cured at 80 ^{o}C for 3 h before use. Then, the opal templates were immersed in 1.0 molL^{-1} $FeCl_3$ solution for 60 s for infiltration and then slowly drawn out. Afterward, the infiltrated sample was kept at 80 ^{o}C and 80% or 30% relative humidity for hydrolysis of infiltrated ferric ions for 30 min.

Finally, the composite opals were calcinated at 450 °C (with 2 °C/min) for 2 h, yielding crack-free hematite inverse opals with a hierarchical matrix. Through solid-state transformation, Fe_3O_4, γ-Fe_2O_3, or FeP crack-free inverse opals could also be obtained. The detailed experiment conditions concerning the solid-state transformation were shown in Figure S7.

Optical and structural characterization:

The photographs of the crack-free hematite inverse opals were taken by a digital camera (Canon EOS 60D). The optical microscope images were taken by Leica DM6M. The reflectance spectra of the inverse opals were measured by a HR 4000 fiber optic UV−vis spectrometer in the reflection mode via a 600 μm broadband optical fiber (Ocean Optics Inc., QP600-1-UV/vis) at normal incident angle to the (111) surface of the inverse opals, with specular reflectance standard (STAN-SSH) as the reference. The UV-vis absorption spectra of the hematite samples were tested on Agilent Cary 5000 UV-Vis-NIR spectrophotometer. The structures of the opal templates and inverse opals were characterized by SEM (Hitachi FE-S4800), coupled with an Inca Energy 350 energy-dispersive X-ray spectroscope (EDS) (Oxford, England). The typical TEM image was taken on JEOL JEM-2100. The crystalline structures of inverse opal samples were characterized by a powder x-ray diffraction (X'Pert PRO, PANalytical, the Netherlands) with a Cu Kα X-ray source. N_2 adsorption-desorption isotherms were obtained at 77 K using a Kubo X1000 apparatus (Beijing Builder Instruments, Beijing, China).

Photoelectrochemical test:

The PEC water splitting performance was tested in a three-electrode configuration with the as-prepared hematite anode as a working electrode (sample area 5 ×5 mm, examined with the optical microscope for cracks to ensure the whole piece was crack-free), Pt as the counter electrode, and

Ag/AgCl as a reference electrode. The photocurrent–voltage curves were measured on an electrochemical workstation (AutoLab PGSTAT302N, Metrohm Autolab BV., Utrecht, the Netherlands), under 250 W xenon lamp solar irradiation supplied by a solar simulator (AM 1.5, SXDN-150E, Panasonic Electric Works SUNX Co., Ltd., China). The incident power was calibrated to be 100 mW/ cm^2 over the irradiation area. EIS measurements were carried out over a frequency range from 100 kHz to 0.1 Hz using the same AutoLab machine under AM 1.5 G light illumination from the solar simulator, with FRA impedance potentiostatic mode. The IPCE was recorded in the wavelength range from 300 to 900 nm by the Zahner Zennium CIMPS-QE/IPCE system (TLS03) using a frequency of 77 Hz.

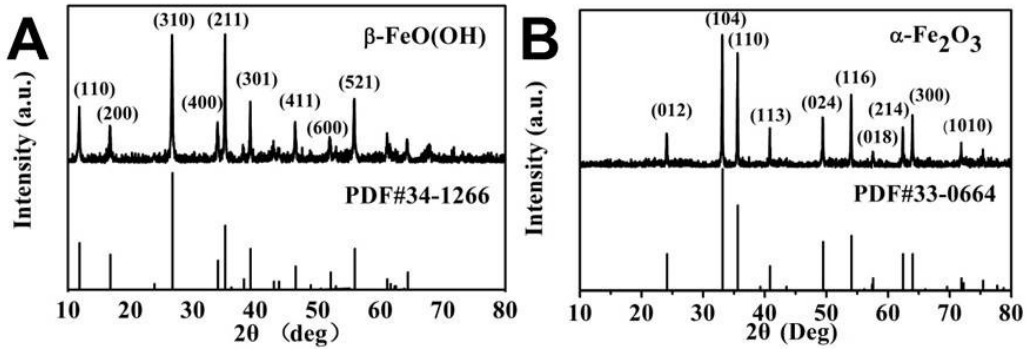

Figure S1. XRD patterns of the samples of (A) obtained from hydrolysis of ferric ions at 80 ^oC and 80% relative humidity and (B) after further calcination. The hydrolysis of ferric ions yielded β-FeO(OH). The final product after calcination was indexed to be hematite (α-Fe_2O_3).

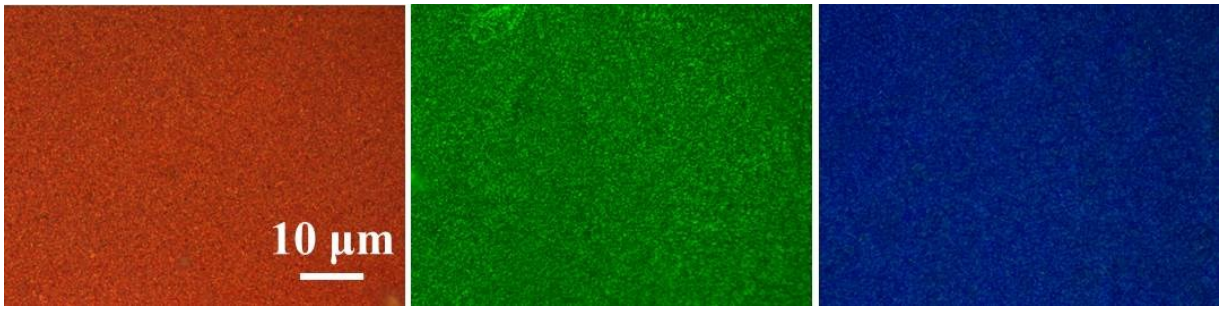

Figure S2. Optical microscope image of typical crack-free hematite inverse opal photo-anodes with red, green, and blue structural colors. No cracks could be observed in the samples under an optical microscope.

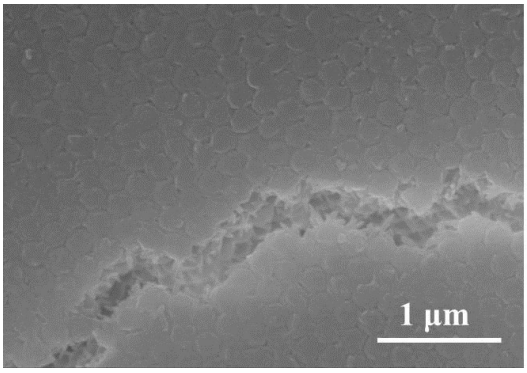

Figure S3. SEM image of the composite opal after hydrolysis of the infiltrated ferric ions at a relative humidity of 30%. The β-FeO(OH) nanoneedles did not grow long enough to bridge to the cracks.

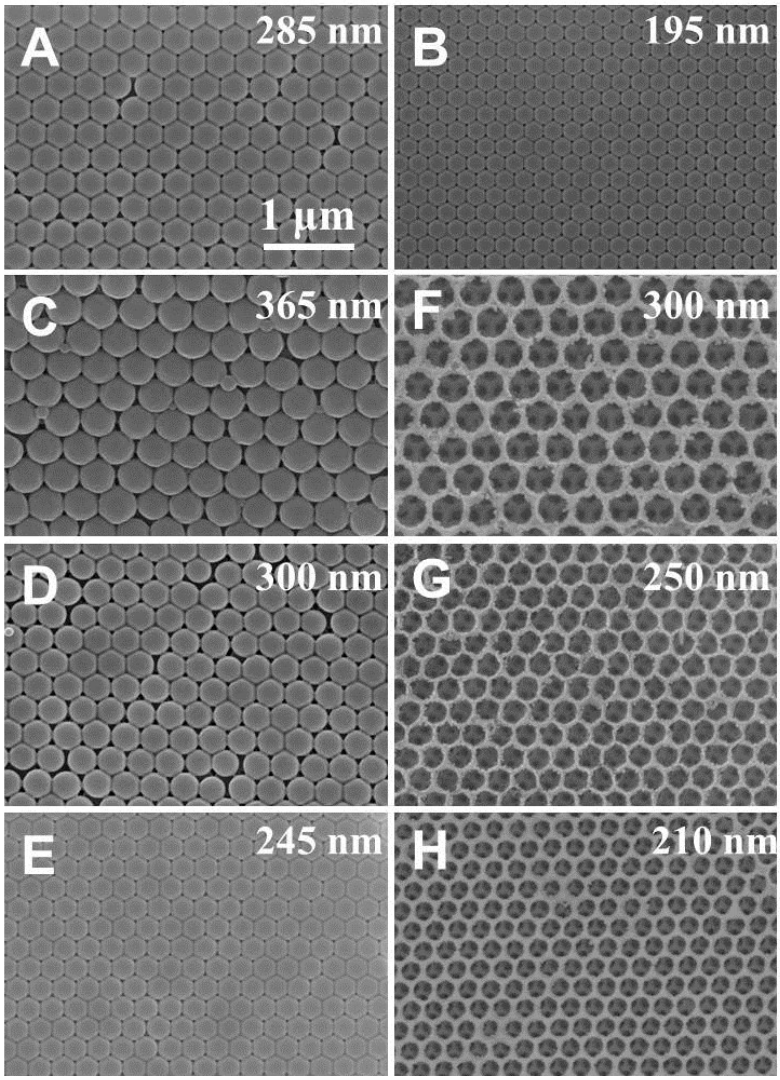

Figure S4. (A), (B) SEM images of the opal templates for producing inverse opals photo-anodes of Figure 3 C and D. (C-E) and (F-H) SEM images of opal templates assembled from latex spheres with various sizes and the corresponding inverse opals with tunable pore sizes, respectively.

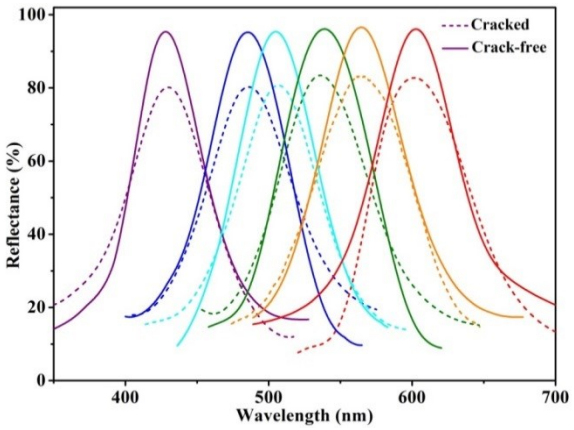

Figure S5. Reflectance spectra of the hematite inverse opal photo-anodes with (dashed lines) and without (solid lines) cracks. The elimination of cracks led to improved reflectivity over 11%, due to the reduced scattering effect caused by the cracks.

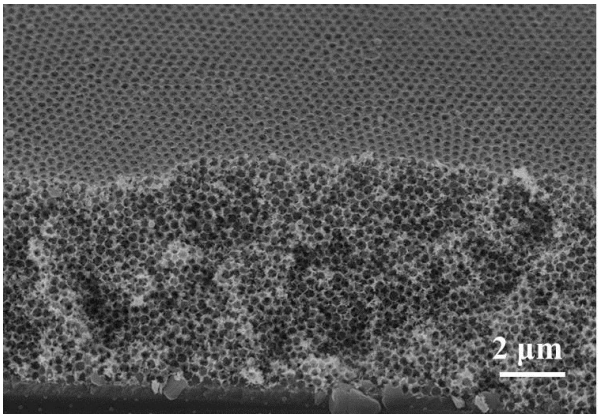

Figure S6. Cross-sectional SEM image of the typical crack-free hematite inverse opal photo-anode.

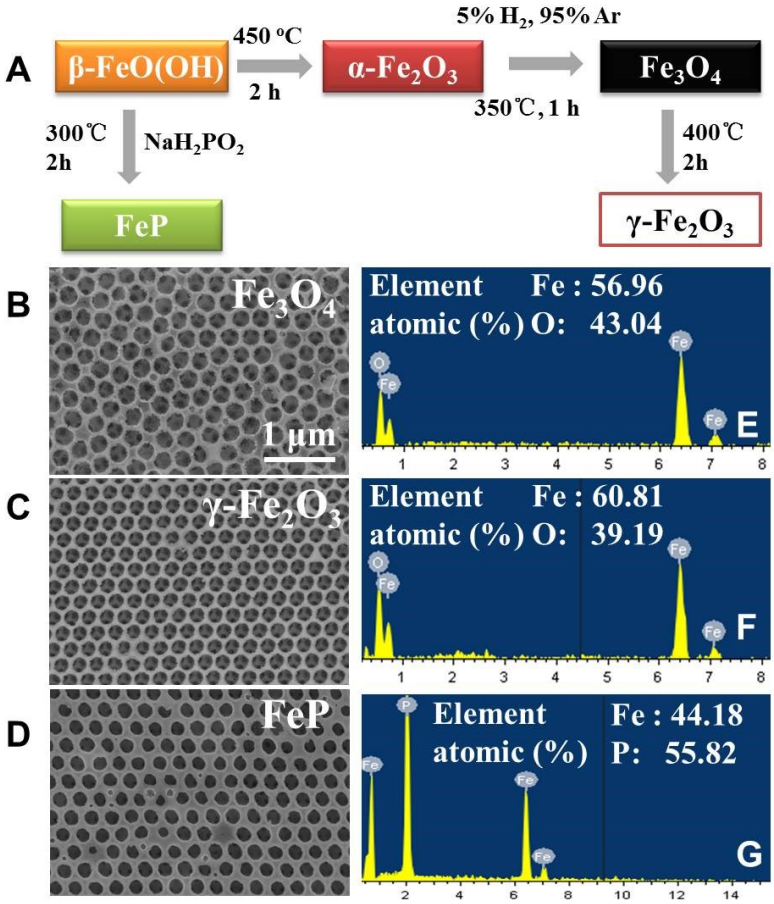

Figure S7. (A) Schematic illustrations of the solid-state transformations of the iron species, which enabled a variety of inverse opal functional matrix. (B), (C), (D) SEM images of crack-free Fe_3O_4, γ-Fe_2O_3, FeP inverse opals obtained through solid-state transformations. (E), (F), (G) The EDX spectra with near stoichiometry to Fe_3O_4, γ-Fe_2O_3, and FeP, respectively.

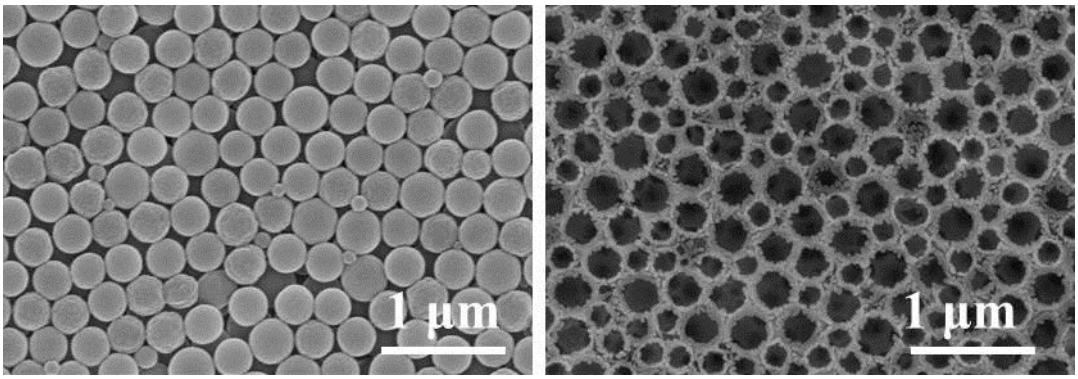

Figure S8. SEM images of the porous hematite photo-anode without PBG and the corresponding amorphous porous photonic structure template.

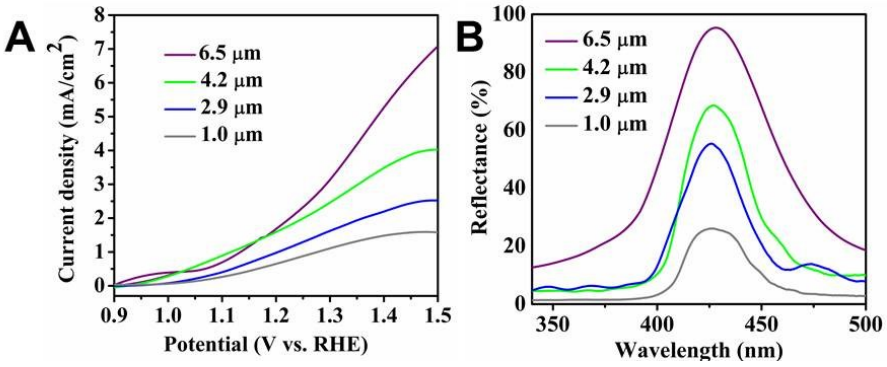

Figure S9. (A) J-V curves and (B) Reflectance spectra of the crack-free hematite inverse opal photo-anodes with varying film thickness. The PBG of the photo-anodes was at ~ 428 nm.

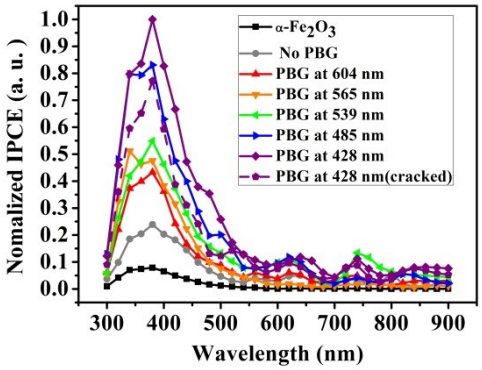

Figure S10. Normalized IPCE of hematite photo-anodes with varying PBG or without PBG.

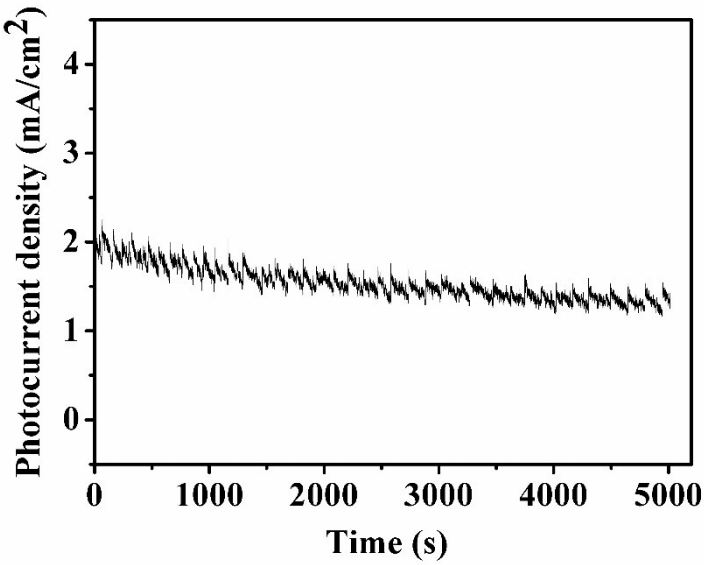

Figure S11. The J-t plot of the photoanodes under a constant bias of 1.23 V vs. RHE and constant illumination of the crack-free inverse opal photo-anodes with a PBG of ~ 428 nm. The photocurrent density retained over 70% of the initial value after nearly 1.4 h, indicating the high stability of the photo-anodes.

Table S1. Summary of the photocurrents and IPCE of the hematite photo-anodes.

Photo-anodes with or without PBG	Photocurrent density at 1.23 V vs RHE (mA/cm^2)	IPCE at 380 nm
428 nm	2.08	19.30%
428 (cracked)	1.49	14.89%
485 nm	1.98	16.04%
539 nm	0.69	10.59%
565 nm	0.81	9.18%
604 nm	0.65	8.36%
Porous (no PBG)	0.28	4.62%
Non-porous (No PBG)	0.18	1.51%

Table S2. The fitting results using the equivalent model for EIS measurements of hematite photo-anodes.

Photo-anodes with or without PBG	R_s (Ω)	R_{ct1} (Ω)	R_{ct2} (Ω)	CPE1 (F)	CPE2 (F)
428 nm	2.49	192.3	213.4	6.9×10^{-3}	9.1×10^{-3}
428 (cracked)	2.273	532	724.6	6.3×10^{-5}	3.0×10^{-4}
485 nm	3.661	209.1	266.1	3.0×10^{-3}	4.9×10^{-4}
539 nm	1.534	205.6	283.8	9.9×10^{-5}	8.9×10^{-5}
565 nm	2.56	233.6	255.6	7.9×10^{-6}	1.3×10^{-4}
604 nm	2.86	271.9	304.8	8.8×10^{-6}	2.3×10^{-5}
Porous (no PBG)	2.661	403.9	1015.0	9.5×10^{-4}	4.0×10^{-4}
Non-porous (No PBG)	1.056	912.4	1293.0	4.6×10^{-3}	3.5×10^{-3}

Table S3. PEC performance of pristine hematite photoanodes and hematite photoanodes with special dopants or conductive matrix. The photocurrent density of the hematite crack-free inverse opal is the highest among the pristine hematite photo-anodes and even superior to many doped anodes.The IPEC at 380 nm varied substantially in the literature and our IPCE value was not the highest, which was probably due to the low absorption at this wavelength (Figure 5A), based on the reduced optical states of the partially overlapping the PBG.

Nanostructures of the hematite based photoanodes	Photocurrent at 1.23 V vs. RHE (mA cm^{-2})	IPCE at 380 nm
Vertically-aligned nanosheets	1.50	~ 28% [S2]
Nanoparticles	1.35	~ 13% [S3]
Ultrathin film	0.70	No data [46]
Nanorods	0.40	2.5%[S3]
Nanorods	1.88	No data[S5]
Nanotube	0.88	~ 2%
Nanotube	1.20	~ 30% [42]
Nanowires	1.24	No data[37]
Nanorods	1.41	~ 65%
Mesoporous	0.56	No data[48]
On antimony-doped SnO_2 inverse opal scaffold	1.28	~ 25%[S6]
Nitrogen-Doped Carbon Nanolayer Coated Hematite Nanorods for	1.76	~ 20% [S7]
Hematite/$NiFeO_x$	~ 0.56	No data [26]
Sn-doped hematite nanocorals	1.86	~ 17% [37]
On $TiSi_2$ nanonet	1.60	No data [41]
ZrO_2-Induced Hematite Nanotube	1.50	~ 26% [44]
ITO@α-Fe_2O_3 Core−Shell Nanowire	1.10	~ 17% [45]
Ultrathin film with TiO_2 underlayer	~ 0.25	~ 15% [47]
Crack-free inverse opal	**~ 2.08**	**~ 19.3% (This work)**

S1 J. X. Wang, Y. Q. Wen, H. L. Ge, Z. W. Sun, Y. M. Zheng, Y. L. Song and L. Jiang, Simple fabrication of full color colloidal crystal films with tough mechanical strength, *Macromol. Chem. Phys.*, 2006, **207**, 596-604.

S2 P. Peerakiatkhajohn, J. H. Yun, H. Chen, M. Lyu, T. Butburee and L. Wang, Stable hematite nanosheet photoanodes for enhanced photoelectrochemical water splitting, *Adv. Mater.*, 2016, **28**, 6405-6410.

S3 Q. Y. Zeng, J. Bai, J. H. Li, L. G. Xia, K. Huang, X. J. Li and B. X. Zhou, A novel in situ preparation method for nanostructured α-Fe_2O_3 films from electrodeposited Fe films for efficient photoelectrocatalytic water splitting and the degradation of organic pollutants, *J. Mater. Chem. A*, 2015, **3**, 4345-4353.

S4 X. Cao, Y. Wang, J. Lin and Y. Ding, Ultrathin CoOx nanolayers derived from polyoxometalate for enhanced photoelectrochemical performance of hematite photoanodes, *J. Mater. Chem. A*, 2019, **7**, 6294-6303.

S5 H. Zhang, J. H. Park, W. J. Byun, M. H. Song and J. S. Lee, Activating the surface and bulk of hematite photoanodes to improve solar water splitting, *Chem. Sci.*, 2019, **10**, 10436-10444.

S6 J. Zhang, J. Li, B. Zhang, J. Ye, Y. Wang and X. Ye, Sn-doped 3D ATO inverse opal/hematite hierarchical structures: facile fabrication and efficient photoelectrochemical performance, *RSC Adv.*, 2018, **8**, 42049-42059.

S7 T.-T. Kong, J. Huang, X.-G. Jia, W.-Z. Wang, Y. Zhou and Z.-G. Zou, Nitrogen-Doped Carbon Nanolayer Coated Hematite Nanorods for Efficient Photoelectrocatalytic Water Oxidation, *Appl. Catal. B: Environ.*, 2020, **275**, 119113.